# Proximity Effect in Graphene–Topological-Insulator Heterostructures

Junhua Zhang, C. Triola, and E. Rossi
*Department of Physics, College of William and Mary, Williamsburg, Virginia 23187, USA*
(Received 3 September 2013; published 4 March 2014)

We formulate a continuum model to study the low-energy electronic structure of heterostructures formed by graphene on a strong three-dimensional topological insulator (TI) for the cases of both commensurate and incommensurate stacking. The incommensurability can be due to a twist angle between graphene and the TI surface or a lattice mismatch between the two systems. We find that the proximity of the TI induces in graphene a strong enhancement of the spin-orbit coupling that can be tuned via the twist angle.

DOI: 10.1103/PhysRevLett.112.096802 PACS numbers: 73.20.-r, 73.22.Pr, 74.45.+c, 75.70.Tj

The surfaces of strong three-dimensional (3D) topological insulators (TIs) [1] and graphene [2,3] have very similar low-energy electronic structures: the conduction and valence bands touch at isolated points, the Dirac points (DP), and around these points the fermionic excitations are well described as massless two-dimensional (2D) chiral Dirac fermions for which the phase of a two-state quantum degree of freedom is locked with the momentum direction. However, there are also qualitative differences: (i) in graphene the chirality is associated with the sublattice degree of freedom whereas in a TI surface (TIS) it is associated with the electron spin; (ii) in graphene the number of DP is even whereas in a TIS it is odd; (iii) in a TI the electron-phonon scattering is much stronger than that in graphene. Therefore, the transport properties of graphene [4] and TIs are different in significant aspects: in graphene, because the intrinsic spin-orbit (SO) coupling is negligible [5–8], no quantum spin Hall effect is expected, contrary to the case in a TI; graphene has the highest room-temperature mobility, whereas TIs have very low mobilities. These facts, together with the recent experimental progress [9], motivated us to study graphene-TI heterostructures, in which the proximity to a TI is expected to enhance the SO coupling of graphene and create a novel 2D system with nontrivial spin textures and high, room-temperature, electron mobility. This approach to enhance the SO coupling in graphene appears to be more practical than previously proposed approaches [10] that rely on doping graphene with heavy adatoms.

In this work, we study the low-energy electronic structure of heterostructures formed by one sheet of graphene placed on the conducting surface of a 3D TI. Our results show that not only can the proximity of a TIS enhance the SO coupling in graphene and bilayer graphene (BLG), but also that this enhancement can be controlled via the relative rotation, the twist angle, between the graphene lattice and the TI's lattice. The presence of a relative rotation, in general, induces an incommensurate stacking of the graphene and the substrate [11] [12–35]. As a consequence we develop and present a theory that is able to take into account the incommensurability between graphene and the TIS. This cannot be achieved via standard approaches, such as density functional theory [36] and tight-binding models, due to the computational cost of these approaches for incommensurate structures. A continuous model, on the other hand, can effectively treat heterostructures with incommensurate stacking. To develop the theory for incommensurate structures, however, we need a continuous model for the commensurate limit. We present such a model and then, starting from it, the model able to treat incommensurate graphene-TI structures. Our results show that in graphene-TI heterostructures the proximity effect induces a strong enhancement of the SO coupling in graphene, nontrivial spin and pseudospin textures on the bands, and that all these effects can be tuned to great extent via the relative rotation between graphene and the TI. Moreover, we present results for the case in which tunneling processes with finite momentum transfer are present.

We consider the TI material to be a tetradymite such as $Bi_2Se_3$, $Bi_2Te_3$, and $Sb_2Te_3$. In these compounds, the surface states are found on the 111 surface. The projected surface Brillouin zone (BZ) is hexagonal with a single DP at the zone center [37]. Let $a_2$ be the effective lattice constant that corresponds to the surface BZ and $a_1 = 2.46$ Å the graphene lattice constant. We have $a_2/(\sqrt{3}a_1) = 1+\delta$ with $\delta < 1\%$ for $Sb_2Te_3$ and $\delta \approx -3\%$ ($\delta \approx +3\%$) for $Bi_2Se_3$ ($Bi_2Te_3$). Thus, the study of the commensurate $\sqrt{3}\times\sqrt{3}$ stacking pattern is expected to be a good approximation for graphene-$Sb_2Te_3$ heterostructure and for developing the theory for incommensurate structures. The Hamiltonian describing the electronic degrees of freedom of the heterostructure can be written as $H = H^g + H^{\mathrm{TIS}} + H_t$, where $H^g$ is the Hamiltonian for an isolated sheet of graphene, $H^{\mathrm{TIS}}$ is the Hamiltonian for the TIS, and $H_t$ describes tunneling processes between graphene and the TIS. The long wavelength physics of graphene is described by a pair of 2D massless Dirac Hamiltonians: $H^{g,K} = \sum_{\mathbf{p},\sigma,\tau\tau'} c^\dagger_{\mathbf{K}+\mathbf{p},\tau,\sigma}(\hbar v_1 \boldsymbol{\tau}\cdot\mathbf{p} - \mu_1)_{\tau\tau'} c_{\mathbf{K}+\mathbf{p},\tau',\sigma}$ and $H^{g,K'} = \sum_{\mathbf{p},\sigma,\tau\tau'} c^\dagger_{\mathbf{K}'+\mathbf{p},\tau,\sigma}(\hbar v_1 \boldsymbol{\tau}^*\cdot\mathbf{p} - \mu_1)_{\tau\tau'} c_{\mathbf{K}'+\mathbf{p},\tau',\sigma}$, where $c^\dagger_{\mathbf{K}+\mathbf{p},\tau,\sigma}$ ($c_{\mathbf{K}+\mathbf{p},\tau,\sigma}$) creates (annihilates) a Dirac fermion on

 © 2014 American Physical Society

sublattice $\tau(A,B)$ with spin $\sigma(\uparrow,\downarrow)$ at a Dirac wave vector $\mathbf{p}$ measured from one of the two inequivalent BZ corners ($K$ and $K'$ valley) located at wave vectors $\mathbf{K}$ and $\mathbf{K}'$ ($|\mathbf{p}| \ll |\mathbf{K}|$), $\boldsymbol{\tau} = (\tau^x, \tau^y)$ are Pauli matrices acting on the sublattice space, $v_1 \approx 10^6$ m/s is the Fermi velocity, and $\mu_1$ is the chemical potential. The TIS states near its Dirac point can be described by an effective 2D continuum model [37,38]: $H^{\mathrm{TIS}} = \sum_{\mathbf{k},\sigma\sigma'} a^\dagger_{\mathbf{k},\sigma}[\hbar v_2(\boldsymbol{\sigma}\times\mathbf{k})\cdot\hat{\mathbf{z}} - \mu_2]_{\sigma\sigma'} a_{\mathbf{k},\sigma'}$, where $a^\dagger_{\mathbf{k},\sigma}$ ($a_{\mathbf{k},\sigma}$) creates (annihilates) a surface massless Dirac fermion with spin $\sigma$ at wave vector $\mathbf{k}$ measured from the zone center ($\bar{\Gamma}$ point), $\boldsymbol{\sigma} = (\sigma^x, \sigma^y)$ are Pauli matrices acting on spin space, $\hat{\mathbf{z}}$ is the unit vector along the $z$ direction, and $\mu_2$ is the chemical potential. In $Bi_2Se_3$, $Bi_2Te_3$, and $Sb_2Te_3$, the Fermi velocity $v_2$ is roughly half of that in graphene; hence, in the remainder we assume $v_2 = v_1/2$. In our model, we neglect the hexagonal warping of the TIS bands due to higher-order terms in $k$ in $H^{\mathrm{TIS}}$ [39]. The reason is that such effects are non-negligible only at relative high energies $\gtrsim$200 meV away from the TI's DP [39,40], and we are only interested in the energy range close to the TI's DP. We also neglect effects due to the TI's bulk states [41] for two reasons: (i) in current experiments the effect of the bulk states can be strongly suppressed via chemical and field effect doping [40,42–44] and by using TI's thin films [45,46]; (ii) the most interesting situation arises when the bulk states can be neglected: in this case, the properties of the systems are dominated not by the TI's bulk states but by the states resulting from the hybridization of the graphene and the TI's surface states. The form of $H_t$ depends on the stacking pattern and the interface properties as we show below.

We first consider the graphene-TI heterostructure in a $\sqrt{3}\times\sqrt{3}$ commensurate stacking, in which each TIS atom is directly underneath a carbon atom. The strongest tunneling is expected to occur between the directly stacked atoms, among which all the carbon atoms can be shown to belong to one sublattice (e.g., sublattice $A$). As a result of the periodic tunneling potential, in the BZ of the heterostructure the original graphene BZ is folded such that the two valleys are both located at the zone center overlapping with the TIS DP; see Figs. 1(a), 1(b). In this case, the tunneling Hamiltonian can be written as $H_t = \sum_{\mathbf{k},\lambda,\tau,\sigma} t_\tau a^\dagger_{\mathbf{k},\sigma} c_{\lambda,\mathbf{k},\tau,\sigma} + \mathrm{H.c.}$, where $\lambda = K$, $K'$ and the tunneling matrix elements $t_A = t$, $t_B = 0$ are assumed to be spin and momentum independent. The Hamiltonian for such a structure takes the form

$$\hat{\mathcal{H}}_{\mathbf{k}} = \begin{pmatrix} \hat{H}^{g,K}_{\mathbf{k}} & 0 & \hat{T}^\dagger \\ 0 & \hat{H}^{g,K'}_{\mathbf{k}} & \hat{T}^\dagger \\ \hat{T} & \hat{T} & \hat{H}^{\mathrm{TIS}}_{\mathbf{k}} \end{pmatrix}, \qquad \hat{T} = \begin{pmatrix} t & 0 & 0 & 0 \\ 0 & 0 & t & 0 \end{pmatrix}, \tag{1}$$

where the graphene blocks are $4\times 4$ matrices in sublattice and spin space whereas the TIS block is a $2\times 2$ matrix in spin space.

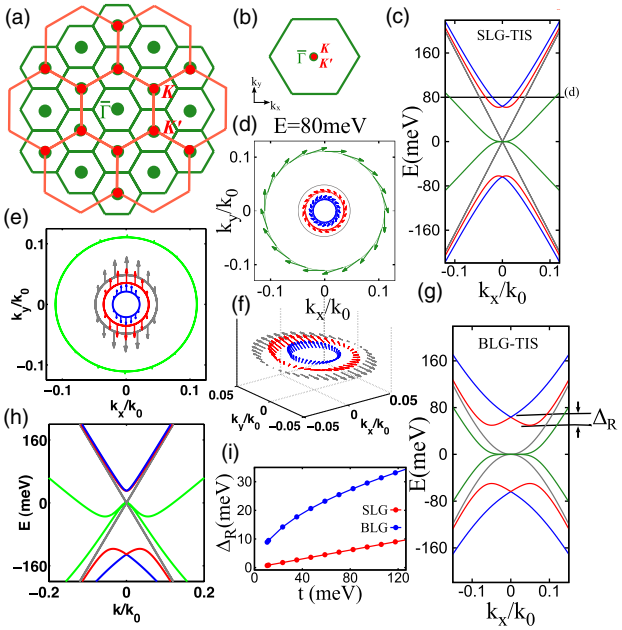


FIG. 1 (color online). (a) Schematics of the $\sqrt{3}\times\sqrt{3}$ stacked graphene BZ (red or dark) and TIS BZ (green or light) in the repeated zone scheme without tunneling. (b) Folded BZ after turning on tunneling. (c) Renormalized bands of SLG-TIS for $\mu_1 = \mu_2 = 0$. Here, $k_0 \equiv 830$ meV$/(\hbar v_2)$. (d) Spin texture on the bands at $E = 80$ meV. The arrows indicate spin directions. (e) Texture of the in-plane component of the pseudospin at $E = 80$ meV and (f) full pseudospin orientation on the three Fermi surfaces closest to the $\bar{\Gamma}$ point. (g) Renormalized bands of BLG-TIS. (h) Renormalized bands of SLG-TIS for $\mu_1 = 0$, $\mu_2 = 100$ meV. (i) Rashba-like splitting $\Delta_R$ in SLG-TIS and BLG-TIS as a function of $t$.

Insights can be achieved using a perturbative approach [47]. In this approach, the effect of tunneling processes on the graphene spectrum is captured by the self-energy $\hat{\Sigma}_{\mathbf{k}}(i\omega_n) = \hat{V}^\dagger \hat{G}^0_{\mathbf{k}}(i\omega_n)\hat{V}$, where $\hat{G}^0_{\mathbf{k}}(i\omega_n)$ is the Green's function of the TIS and $\hat{V}$ is the tunneling vertex. In the basis formed by the eigenstates of the Hamiltonian of isolated graphene $\Phi_{\lambda,\mathbf{k},\alpha,\sigma}$, where $\alpha = \pm$ refer to the four-fold degenerate upper and lower bands, we obtain

$$\hat{\Sigma}_{\mathbf{k}}(i\omega_n) = \begin{pmatrix} \Sigma^S_{\mathbf{k}}(i\omega_n) & e^{-i(\theta_{\mathbf{k}}-(\pi/2))}\Sigma^A_{\mathbf{k}}(i\omega_n) \\ e^{i(\theta_{\mathbf{k}}-(\pi/2))}\Sigma^A_{\mathbf{k}}(i\omega_n) & \Sigma^S_{\mathbf{k}}(i\omega_n) \end{pmatrix} \otimes (I_\alpha + \sigma^x_\alpha) \otimes (I_\lambda + \sigma^x_\lambda), \tag{2}$$

where $\Sigma^{S/A}_{\mathbf{k}}(i\omega_n) = (t^2/2)G^{S/A}_{\mathbf{k}}(i\omega_n)$ with $G^{S/A}_{\mathbf{k}}(i\omega_n) = [1/(i\omega_n - \hbar v_2 k + \mu_2) \pm 1/(i\omega_n + \hbar v_2 k + \mu_2)]/2$, and the first $2\times 2$ matrix acts in the spin space, $(I_\alpha + \sigma^x_\alpha)$ acts in the band space, and $(I_\lambda + \sigma^x_\lambda)$ acts in the valley space. $I$ is the $2\times 2$ identity matrix, and $\theta_{\mathbf{k}} = \arctan(k_y/k_x)$. The appearance of nonzero off-diagonal spin components with phase factor $[\theta_{\mathbf{k}} - (\pi/2)]$ in the self-energy indicates an induced helical spin texture on some of the graphene bands. The renormalized graphene bands in the perturbative approach coincide with those obtained by direct diagonalization.

Figure 1(c) shows the band structure of a graphene-TI heterostructure with $t = 45$ meV and $\mu_1 = \mu_2 = 0$. We see that the fourfold degeneracy of the original graphene bands is partially lifted. In our model the eigenstates of the hybridized bands can be calculated explicitly. This allows us to (i) obtain directly both the spin and *pseudospin* configuration on all the renormalized bands, Figs. 1(d)–1(f); (ii) show that, as expected from the form of the self-energy, on the two gapped bands (forming the two smaller Fermi surfaces) the in-plane spin is locked perpendicular to the momentum and winds around the $\bar{\Gamma}$ point either clockwise or counterclockwise, analogous to a system with Rashba-type SO coupling, Fig. 1(d); (iii) show that the spin helicity of the hybridized bands can be different (opposite) to the helicity of the original TI's band, Fig. 1(d); (iv) show that the two degenerate bands, seemingly equal to the original graphene (or BLG) bands, are in reality antisymmetric combinations of the states of isolated graphene (or BLG) at opposite valleys $(1/\sqrt{2})(\Phi_{K,\alpha,\uparrow} - \Phi_{K',\alpha,\uparrow})$ and $(1/\sqrt{2})(\Phi_{K,\alpha,\downarrow} - \Phi_{K',\alpha,\downarrow})$, $\alpha = \pm$; and (v) show that the two degenerate bands have a unique pseudospin structure, very different from the pseudospin structure of both the original $K$ and $K'$ valleys, which we expect would affect transport measurements, Figs. 1(e), 1(f). In addition, our model is easily generalized to the case of BLG. The results of Fig. 1(g) show the bands of a BLG-TI heterostructure and reveal that the enhancement, due to the proximity effect, of the SO coupling in BLG is much larger than in single layer graphene (SLG), Fig. 1(i). This is due mostly to the fact that, at low energies, BLG has a much higher density of states (DOS) than SLG. Finally, we consider the effect of a difference $\delta\mu = \mu_2 - \mu_1$ between the TI's and graphene chemical potential. By varying $\delta\mu$ the value of $\mathbf{k}$ for which the pristine bands of the TI and graphene cross and for which the hybridization is stronger can be tuned. Figure 1(h) shows the case for which $\mu_2 = 100$ meV and $\mu_1 = 0$. We see that in this case the induced Rashba splitting is stronger than when $\mu_2 = \mu_2 = 0$. This is due to the fact that the density of states increases as we move away from the DP.

We now consider incommensurate structures. The tunneling matrix elements can be written as

$$T_\tau(\mathbf{k}_2, \mathbf{k}_1) = \sum_{\mathbf{G}_1,\mathbf{G}_2} \frac{t(\mathbf{k}_1 + \mathbf{G}_1)}{\sqrt{3}\Omega_1} e^{i\mathbf{G}_1\cdot\mathbf{d}_\tau} \delta_{\mathbf{k}_2+\mathbf{G}_2,\mathbf{k}_1+\mathbf{G}_1} \quad (3)$$

where the crystal momentum is conserved by the tunneling process in which a graphene quasiparticle of wave vector $\mathbf{k}_1$ residing on sublattice $\tau$ hops to a TIS state with wave vector $\mathbf{k}_2$. $\Omega_1$ is the graphene unit cell area, and $\mathbf{d}_A = \mathbf{0}$, $\mathbf{d}_B = (-a_0, 0)$ are the positions of the two carbon atoms in a unit cell with carbon-carbon distance $a_0$. $\{\mathbf{G}_1\}$, $\{\mathbf{G}_2\}$ are the reciprocal lattice vectors of graphene and TIS, respectively. $t(\mathbf{k})$ are the Fourier amplitudes of the tunneling potential $t(\mathbf{r})$ assumed to be a smooth function of $\mathbf{r}$, the spatial separation between graphene and TIS atoms projected onto the interface plane. Given that the graphene-TIS separation distance

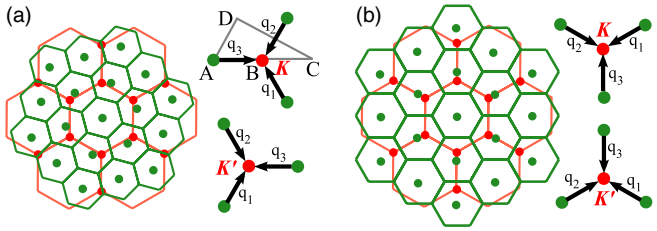


FIG. 2 (color online). Schematics of the graphene and TIS BZs in an incommensurate structure formed from (a) a twist and (b) a lattice mismatch, with the corresponding $\mathbf{q}_j$ vectors at the $K$ and $K'$ points.

exceeds the interatomic distance in each material, the dominant tunneling amplitudes of $t(\mathbf{k})$ near the graphene DP are the ones with $|\mathbf{k}| = K_D \equiv |\mathbf{K}|$. This allows us to restrict the sum over $\{\mathbf{G}_1\}$ to three vectors: $\mathbf{g}_1 (= \mathbf{0})$, $\mathbf{g}_2$, $\mathbf{g}_3$, where the latter two connect a valley with its equivalent first BZ corners. For small wave vectors measured from the respective DP, we have $H_t = \sum_{\mathbf{p},\tau,\sigma} \sum_{j,l,\ldots=1}^{3} [T_{\tau,j} a^\dagger_{\mathbf{p}+\mathbf{q}_j,\sigma} c_{\mathbf{p},\tau,\sigma} + T^*_{\tau,l} c^\dagger_{\mathbf{p}+\mathbf{q}_j+\bar{\mathbf{q}}_l,\tau,\sigma} a_{\mathbf{p}+\mathbf{q}_j,\sigma} + \ldots]$, where $T_{\tau,j} = t' e^{i\mathbf{g}_j\cdot\mathbf{d}_\tau}$ with $t' \equiv t(K_D)/(\sqrt{3}\Omega_1)$, $\{\mathbf{q}_j\}$ are the offset vectors between the graphene DP and the three "nearest-neighboring" TIS DP, and $\bar{\mathbf{q}}_l \in \{-\mathbf{q}_j\}$, as shown in Fig. 2. The repeated action of the "nonlocal" coupling generates a $k$-space lattice [20]. For a rotation angle $\theta$, the separation between the offset DP is $|\mathbf{q}_j| \equiv q = 2K_D \sin(\theta/2)$, for the lattice mismatch case, $q = |\delta/(1+\delta)|K_D$, Fig. 2.

For very small twist angles or lattice mismatches such that the dimensionless parameter $\gamma \equiv t'/(\hbar v_2 q) > 1$, graphene and TIS will be strongly coupled. However, when $\gamma < 1$, a weak coupling theory is valid [12,20,22]. In this case, to investigate the low-energy spectrum of graphene, we can truncate the $k$-space lattice and obtain the Hamiltonian

$$\hat{\mathcal{H}}_{\mathbf{p}} = \begin{pmatrix} \hat{H}^{g,K}_{\mathbf{p}} & \hat{T}^\dagger_1 & \hat{T}^\dagger_2 & \hat{T}^\dagger_3 \\ \hat{T}_1 & \hat{H}^{\mathrm{TIS}}_{\mathbf{q}_1+\mathbf{p}} & 0 & 0 \\ \hat{T}_2 & 0 & \hat{H}^{\mathrm{TIS}}_{\mathbf{q}_2+\mathbf{p}} & 0 \\ \hat{T}_3 & 0 & 0 & \hat{H}^{\mathrm{TIS}}_{\mathbf{q}_3+\mathbf{p}} \end{pmatrix},$$

$$\hat{T}_1 = \begin{pmatrix} t' & t' & 0 & 0 \\ 0 & 0 & t' & t' \end{pmatrix},$$

$$\hat{T}_2 = \begin{pmatrix} t' & t' e^{-i(2\pi/3)} & 0 & 0 \\ 0 & 0 & t' & t' e^{-i(2\pi/3)} \end{pmatrix},$$

$$\hat{T}_3 = \begin{pmatrix} t' & t' e^{i(2\pi/3)} & 0 & 0 \\ 0 & 0 & t' & t' e^{i(2\pi/3)} \end{pmatrix}. \quad (4)$$

A similar Hamiltonian is valid for the $K'$ valley [48]. In the absence of twist and mismatch, the system reduces to the commensurate structure, giving rise to $\hat{T} = \hat{T}_1 + \hat{T}_2 + \hat{T}_3$ so that $t' = t/3$.

Figures 3(a)–3(c) show the band and spin structure around the $K$ point for an incommensurate graphene-TI

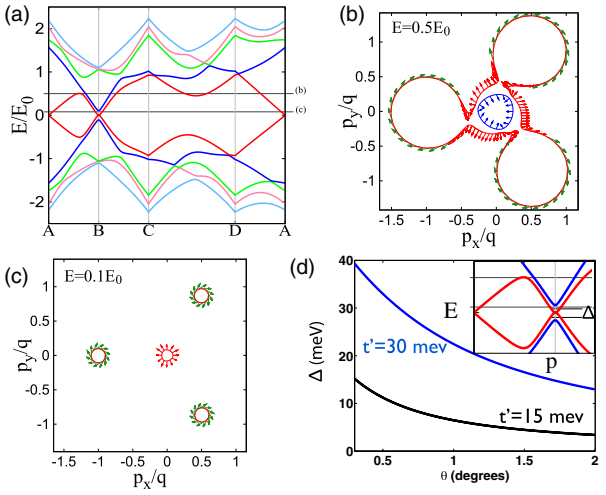


FIG. 3 (color online). (a) The band structure along the path *A-B-C-D-A* indicated in Fig. 2(a). [(b),(c)] Spin texture on the bands at different energies; $E_0 \equiv \hbar v_2 q = t'/\gamma$. (d) Splitting ($\Delta$) of the low-energy bands as a function of twist angle for $t' = 30$ meV and $t' = 15$ meV.

heterostructure with $\gamma = 0.2$, $t' = 15$ meV, and $\mu_1 = \mu_2 = 0$. The result for the $K'$ point is simply a 60° rotation of the former. The results of Fig. 3 show that (i) the original twofold spin degeneracy of the graphene Dirac cone is completely lifted; (ii) of the two original degenerate linear bands one is now fully gapped and the other is no longer linear at the DP; (iii) the bands acquire nontrivial in-plane spin textures. The key property of graphene-TI heterostructures is that the features of the band structure and spin texture can be controlled via the twist angle. By changing the value of $\theta$, for fixed $t'$ and energy, the distance between the Fermi pockets shown in Figs. 3(b) and 3(c) and their size can be tuned. In addition, the splitting of the low-energy bands $\Delta$ can be controlled as shown in Fig. 3(d).

In the presence of surface roughness and/or phonons tunneling processes with finite momentum transfer are allowed. We expect the effect of such processes to be weak; however, to gain some insight, we consider the case in which the tunneling amplitude has a Gaussian profile with respect to the momentum transfer $\mathbf{q}$: $t_{\mathbf{q}} = t_0 \exp(-|\mathbf{q}|^2/(2\sigma^2))$, where $t_0$ characterizes the tunneling strength and $\sigma$ the variance. To qualitatively understand the effect of such processes, we study the case of an isolated graphene Dirac cone separated by a large wave vector $\mathbf{Q}$ from the closest TIS DP. With the use of the perturbative approach outlined above, the proximity effect on the graphene spectrum is captured by the self-energy

$$\hat{\Sigma}_{\mathbf{Q}+\mathbf{p}}(i\omega_n) = (I_\alpha + \sigma_\alpha^x) \otimes \begin{pmatrix} \Sigma^S_{\mathbf{Q}+\mathbf{p}}(i\omega_n) & e^{-i(\theta_{\mathbf{Q}+\mathbf{p}}-\pi/2)}\Sigma^A_{\mathbf{Q}+\mathbf{p}}(i\omega_n) \\ e^{i(\theta_{\mathbf{Q}+\mathbf{p}}-\pi/2)}\Sigma^A_{\mathbf{Q}+\mathbf{p}}(i\omega_n) & \Sigma^S_{\mathbf{Q}+\mathbf{p}}(i\omega_n) \end{pmatrix} \quad (5)$$

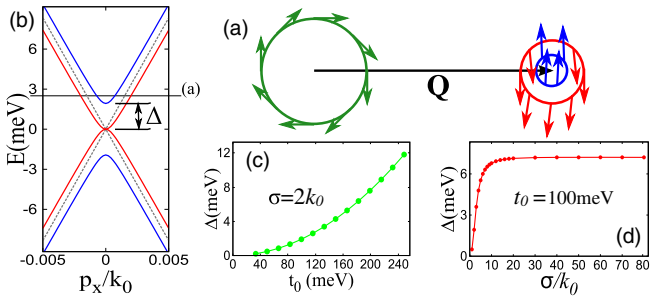


FIG. 4 (color online). (a) Schematics of the induced spin texture on graphene (right) from the TIS spin helix (left). (b) Renormalized graphene bands (solid lines) for $t_0 = 100$ meV, $\sigma = 2k_0$. Spin-split gap ($\Delta$) as a function of (c) $t_0$ and (d) $\sigma$.

with

$$\Sigma^{S/A}_{\mathbf{Q}+\mathbf{p}}(i\omega_n) = \frac{t_0^2\Omega_2}{2\pi}\exp\left[-\frac{|\mathbf{Q}+\mathbf{p}|^2}{\sigma^2}\right]\int_0^\infty k\exp\left[-\frac{k^2}{\sigma^2}\right] \times I_{0/1}\left(\frac{2|\mathbf{Q}+\mathbf{p}|}{\sigma^2}k\right)G^{S/A}_{\mathbf{k}}(i\omega_n)dk,$$

where $I_n(x)$, $n = 0, 1$ are the modified Bessel functions of the first kind. The form of the phase factors in the off-diagonal spin components of $\hat{\Sigma}$ implies an induced spin texture on graphene with the spin perpendicular to the wave vector $\mathbf{Q} + \mathbf{p}$, Fig. 4(a). We find, Fig. 4(b), that also in this case the spin degenerate bands are split and the remaining gapless bands are no longer linear. Figures 4(c) and 4(d) show the size of the gap between spin-split bands as a function of $t_0$ and $\sigma$, respectively.

In conclusion, we have studied the proximity effect of a strong 3D TI on the low-energy spectrum of graphene in commensurate and incommensurate structures as well as in a case with surface roughness. To be able to take into account the incommensurability, we have developed a continuous model. Using this model we have been able to identify, both for commensurate and incommensurate stacking, the spin and pseudospin structure of all the hybridized bands and show that it is very unusual and likely to affect transport measurements. We have also shown that the enhancement of the SO coupling is in general much stronger in BLG than in graphene. In addition, we have shown that properties of these bands and their spin structures can be substantially tuned by varying the relative rotation between the graphene lattice and the TI's lattice.

We acknowledge helpful discussions with Michael Fuhrer and Elsa Prada. This work is supported by ONR, Grant No. ONR-N00014-13-1-0321, ACS-PRF No. 53581-DNI5, and the Jeffress Memorial Trust. C. T. acknowledges support from the Virginia Space Grant Consortium.

[1] M. Z. Hasan and C. L. Kane, Rev. Mod. Phys. **82**, 3045 (2010).
[2] K. S. Novoselov, A. K. Geim, S. V. Morozov, D. Jiang, Y. Zhang, S. V. Dubonos, I. V. Grigorieva, and A. A. Firsov, Science **306**, 666 (2004).

[3] A. H. C. Neto, F. Guinea, N. M. R. Peres, K. S. Novoselov, and A. K. Geim, Rev. Mod. Phys. **81**, 109 (2009).

[4] S. Das Sarma, S. Adam, E. H. Hwang, and E. Rossi, Rev. Mod. Phys. **83**, 407 (2011).

[5] H. Min, J. E. Hill, N. A. Sinitsyn, B. R. Sahu, L. Kleinman, and A. H. MacDonald, Phys. Rev. B **74**, 165310 (2006).

[6] Y. G. Yao, F. Ye, X. L. Qi, S. C. Zhang, and Z. Fang, Phys. Rev. B **75**, 041401 (2007).

[7] M. Gmitra, S. Konschuh, C. Ertler, C. Ambrosch-Draxl, and J. Fabian, Phys. Rev. B **80**, 235431 (2009).

[8] E. I. Rashba, Phys. Rev. B **79**, 161409 (2009).

[9] W. H. Dang, H. L. Peng, H. Li, P. Wang, and Z. F. Liu, Nano Lett. **10**, 2870 (2010); C.-L. Song, Y.-L. Wang, Y.-P. Jiang, Y. Zhang, C.-Z. Chang, L. Wang, K. He, X. Chen, J.-F. Jia, Y. Wang *et al.*, Appl. Phys. Lett. **97**, 143118 (2010).

[10] C. Weeks, J. Hu, J. Alicea, M. Franz, and R. Wu, Phys. Rev. X **1**, 021001 (2011); H. Jiang, Z. H. Qiao, H. W. Liu, J. R. Shi, and Q. Niu, Phys. Rev. Lett. **109**, 116803 (2012).

[11] K. S. Novoselov, D. Jiang, F. Schedin, T. J. Booth, V. V. Khotkevich, S. V. Morozov, and A. K. Geim, Proc. Natl. Acad. Sci. U.S.A. **102**, 10451 (2005); S. Kim, J. Nah, I. Jo, D. Shahrjerdi, L. Colombo, Z. Yao, E. Tutuc, and S. K. Banerjee, Appl. Phys. Lett. **94**, 062107 (2009); S. Kim, I. Jo, J. Nah, Z. Yao, S. K. Banerjee, and E. Tutuc, Phys. Rev. B **83**, 161401 (2011); L. A. Ponomarenko, A. K. Geim, A. A. Zhukov, R. Jalil, S. V. Morozov, K. S. Novoselov, I. V. Grigorieva, E. H. Hill, V. V. Cheianov, V. I. Fal'Ko *et al.*, Nat. Phys. **7**, 958 (2011); S. Kim and E. Tutuc, Solid State Commun. **152**, 1283 (2012); R. V. Gorbachev, A. K. Geim, M. I. Katsnelson, K. S. Novoselov, T. Tudorovskiy, I. V. Grigorieva, A. H. MacDonald, S. V. Morozov, K. Watanabe, T. Taniguchi *et al.*, Nat. Phys. **8**, 896 (2012); S. J. Haigh, A. Gholinia, R. Jalil, S. Romani, L. Britnell, D. C. Elias, K. S. Novoselov, L. A. Ponomarenko, A. K. Geim, and R. Gorbachev, Nat. Mater. **11**, 764 (2012); J. Zhang and E. Rossi, Phys. Rev. Lett. **111**, 086804 (2013).

[12] J. M. B. Lopes dos Santos, N. M. R. Peres, and A. H. Castro Neto, Phys. Rev. Lett. **99**, 256802 (2007).

[13] E. J. Mele, Phys. Rev. B **81**, 161405 (2010).

[14] S. Shallcross, S. Sharma, E. Kandelaki, and O. A. Pankratov, Phys. Rev. B **81**, 165105 (2010).

[15] E. Suárez Morell, J. D. Correa, P. Vargas, M. Pacheco, and Z. Barticevic, Phys. Rev. B **82**, 121407 (2010).

[16] R. Bistritzer and A. H. MacDonald, Phys. Rev. B **81**, 245412 (2010).

[17] J. Li, I. Martin, M. Buttiker, and A. F. Morpurgo, Nat. Phys. **7**, 38 (2011).

[18] E. J. Mele, Phys. Rev. B **84**, 235439 (2011).

[19] R. Bistritzer and A. H. MacDonald, Phys. Rev. B **84**, 035440 (2011).

[20] R. Bistritzer and A. H. MacDonald, Proc. Natl. Acad. Sci. U.S.A. **108**, 12233 (2011).

[21] E. Suárez Morell, P. Vargas, L. Chico, and L. Brey, Phys. Rev. B **84**, 195421 (2011).

[22] E. J. Mele, J. Phys. D **45**, 154004 (2012).

[23] M. Kindermann and E. J. Mele, Phys. Rev. B **84**, 161406 (2011).

[24] A. Luican, G. Li, A. Reina, J. Kong, R. R. Nair, K. S. Novoselov, A. K. Geim, and E. Y. Andrei, Phys. Rev. Lett. **106**, 126802 (2011).

[25] W. Yan, M. Liu, R.-F. Dou, L. Meng, L. Feng, Z.-D. Chu, Y. Zhang, Z. Liu, J.-C. Nie, and L. He, Phys. Rev. Lett. **109**, 126801 (2012).

[26] J. D. Sanchez-Yamagishi, T. Taychatanapat, K. Watanabe, T. Taniguchi, A. Yacoby, and P. Jarillo-Herrero, Phys. Rev. Lett. **108**, 076601 (2012).

[27] P. San-Jose and E. Prada, Phys. Rev. B **88**, 121408(R) (2013).

[28] C.-K. Lu and H. A. Fertig, arXiv:1308.1962 [Phys. Rev. B (to be published)].

[29] C. R. Dean, A. F. Young, I. Meric, C. Lee, L. Wang, S. Sorgenfrei, K. Watanabe, T. Taniguchi, P. Kim, K. L. Shepard *et al.*, Nat. Nanotechnol. **5**, 722 (2010).

[30] J. Xue, J. Sanchez-Yamagishi, D. Bulmash, P. Jacquod, A. Deshpande, K. Watanabe, T. Taniguchi, P. Jarillo-Herrero, and B. J. Leroy, Nat. Mater. **10**, 282 (2011).

[31] M. Yankowitz, J. Xue, D. Cormode, J. D. Sanchez-Yamagishi, K. Watanabe, T. Taniguchi, P. Jarillo-Herrero, P. Jacquod, and B. J. Leroy, Nat. Phys. **8**, 382 (2012).

[32] L. A. Ponomarenko, R. V. Gorbachev, G. L. Yu, D. C. Elias, R. Jalil, A. A. Patel, A. Mishchenko, A. S. Mayorov, C. R. Woods, J. R. Wallbank *et al.*, Nature (London) **497**, 594 (2013).

[33] B. Hunt, J. D. Sanchez-Yamagishi, A. F. Young, M. Yankowitz, B. J. LeRoy, K. Watanabe, T. Taniguchi, P. Moon, M. Koshino, P. Jarillo-Herrero *et al.*, Science **340**, 1427 (2013).

[34] C. R. Dean, L. Wang, P. Maher, C. Forsythe, F. Ghahari, Y. Gao, J. Katoch, M. Ishigami, P. Moon, M. Koshino *et al.*, Nature (London) **497**, 598 (2013).

[35] M. Mucha-Kruczynski, J. Wallbank, and V. I. Fal'ko, Phys. Rev. B **88**, 205418 (2013).

[36] K.-H. Jin and S.-H. Jhi, Phys. Rev. B **87**, 075442 (2013).

[37] H. J. Zhang, C. X. Liu, X. L. Qi, X. Dai, Z. Fang, and S. C. Zhang, Nat. Phys. **5**, 438 (2009).

[38] C.-X. Liu, X.-L. Qi, H. J. Zhang, X. Dai, Z. Fang, and S.-C. Zhang, Phys. Rev. B **82**, 045122 (2010).

[39] L. Fu, Phys. Rev. Lett. **103**, 266801 (2009).

[40] J.-H. Chen, W. G. Cullen, C. Jang, M. S. Fuhrer, and E. D. Williams, Phys. Rev. Lett. **102**, 236805 (2009).

[41] J. G. Analytis, J. H. Chu, Y. L. Chen, F. Corredor, R. D. McDonald, Z. X. Shen, and I. R. Fisher, Phys. Rev. B **81**, 205407 (2010).

[42] D. Hsieh, Y. Xia, D. Qian, L. Wray, F. Meier, J. H. Dil, J. Osterwalder, L. Patthey, A. V. Fedorov, H. Lin *et al.*, Phys. Rev. Lett. **103**, 146401 (2009).

[43] H. Steinberg, D. R. Gardner, Y. S. Lee, and P. Jarillo-Herrero, Nano Lett. **10**, 5032 (2010).

[44] J. G. Checkelsky, Y. S. Hor, R. J. Cava, and N. P. Ong, Phys. Rev. Lett. **106**, 196801 (2011).

[45] Y. Zhang, K. He, C.-Z. Chang, C.-L. Song, L.-L. Wang, X. Chen, J.-F. Jia, Z. Fang, X. Dai, W.-Y. Shan *et al.*, Nat. Phys. **6**, 584 (2010).

[46] A. A. Taskin, S. Sasaki, K. Segawa, and Y. Ando, Phys. Rev. Lett. **109**, 066803 (2012).

[47] J. A. Hutasoit and T. D. Stanescu, Phys. Rev. B **84**, 085103 (2011).

[48] Note that the Dirac Hamiltonian of graphene in the sublattice basis has a phase factor on the off-diagonal terms to take into account a rotational transformation of coordinates due to the choice of the current BZ orientation.